Model-Based Diagnostics and Prognostics for Solid Rocket Motors

Dmitry G. Luchinsky[1], Viatcheslav V. Osipov[2], Vadim N. Smelyanskiy[3], A. Patterson-Hine[4], Ben Hayashida[5], Michael Watson[6], Joshua McMillin[7], David Shook[8], Mont Johnson[9], Scott Hyde[10]

[1,2] *Mission Critical Technologies Inc., 2041Rosecrans Ave. Suite 225 El Segundo, CA 90245*

Dmitry.G.Luchinsky@nasa.gov
Viatcheslav.V.Osipov@nasa.gov

[3,4] *NASA Ames Research Center, Mail Stop 269-2, Moffett Field, CA 94035, USA*

Vadim.N.Smelyanskiy@nasa.gov
Ann.Patterson-Hine@nasa.gov

[5,6] NASA Marshall Space Flight Center, Huntsville, Alabama 35812

Ben.Hayashida@nasa.gov
Michael.D.Watson@nasa.gov

[7,8,9,10] *ATK Thiokol, Large Salt Lake City Area, Utah*

Mont.Johnson@ATK.com
David.Shook@ATK.com
Joshua.McMillin@nasa.gov
Scott.Hyde@nasa.gov

ABSTRACT(MODIFIED)

Progress in development of the physics model based diagnostic and prognostic system for solid rocket motors (SRMs) of the new generation of the crew exploration vehicles is reported. The performance model (PM) of the internal ballistics of large segmented SRMs in the regime of steady burning in the presence of the case breach fault is presented. This model takes into account propellant regression, erosive burning, surface friction, nozzle ablation, and also processes describing specific faults. The performance of the model is verified by comparison with the results of 2D high-fidelity simulations. Importantly, the PM allows for the simulation of a number of faults observed earlier in large segmented SRMs including nozzle blocking, bore choking, propellant debonding, and case breach fault. The developed model of the case breach allows calculations of the side thrust at a given location along the rocket axis. The model takes into account the effect of mass addition along the rocket axis, erosive burning, and surface friction.

In this paper we illustrate to use the developed PM for analysis of the case breach fault. The model of the internal ballistics is combined with the model of dynamics of burning-through case at a given location along the motor axis. The case breach fault diagnostic is developed via inference of the case breach area in a quasi-steady approximation. Prognosis of the case breach fault is achieved using a scaling algorithm. The diagnostic and prognostic algorithms were verified using the results of a ground firing test of a sub-scale motor.*

NOMENCLATURE

ρ = gas density
p = gas pressure
p_0 = gas pressure at the chamber head
p_{ns} = nozzle stagnation pressure
T = gas temperature
u = gas velocity
c = sound velocity
M = Mach number, $M = u/c$, $M_0 = u/c_0$
C_V = specific heat for the constant volume
C_P = specific heat for the constant pressure
γ = ration of specific heats; $\gamma = C_p/C_V$
l = perimeter of the burning propellant surface
L = length of the propellant grain
L_0 = typical length equal to 1m
L_h = perimeter of the hole cross-section
R = burn distance of the propellant
R_t = radius of the nozzle throat
R_{ex} = radius of the nozzle exit
R_h = radius of the hole throat
A_p = cross-section of propellant surface
A_t = cross-sectional area of the nozzle throat
A_h = cross-sectional area of the hole throat
e_T = total energy of the combustion gas
h_T = total enthalpy of the combustion
F_h = additional thrust produced by hole gas flow
F_N = normal thrust
r_c = reference burning rate
r_b = burning rate of solid propellant
r_{er} = erosive burning rate of solid propellant
n = exponent for burning rate of the propellant
a = constant for burning rate [$a = r_c/p_c^n$]
p_c = reference pressure for burning rate
ρ_p = density of the solid propellant
H = combustion heat of the solid propellant
I = variable in the Vilyunov correlation law
j = mass flow density [$j = u\rho$]
J = mass flow [$J = u\rho S$]
h = heat transfer coefficient
Q = heat flow from the gas to a hole wall
f_{tr} = surface friction force
v_h = velocity of propagation of hole wall
v_{abl} = velocity of propagation of ablation front
$v_{m,t}$ = typical ablation velocity of nozzle throat
$v_{m,ex}$ = typical ablation velocity of nozzle exit
Q_c = convection heat flow
Q_R = radiation heat flow
T_{mel} = melting temperature point
H_{met} = heat of combustion of case metal
T_b = temperature of metal surface burning
T_{abl} = characteristic temperature of ablation
T_{m0} = temperature of metal far from hole
C_{met} = specific heat of case metal
q_{met} = specific melting heat of case metal
C_{ins} = specific heat of insulator layer
q_{ins} = specific ablation heat of insulator layer
ρ_{met} = density of case metal
ρ_{ins} = density of insulator layer
k = the thermal conductivity
μ = dynamical viscosity of hot gas

Subscripts:
S = stagnation gas
in = initial states
i = i-part of the ballistic element
h = parameters in the hole
ex = parameters in the nozzle exit
t = parameters in the nozzle throat
nr = parameters in the nominal regime
N = parameters in the nozzle
0 = parameters at the chamber head
L = parameters at the grain outlet (nozzle inlet)
A = parameters at the aft end

1. INTRODUCTION

Development of an in-flight Failure Detection and Prognostic (FD&P) system for SRMs is a prerequisite for the safe exploitation of the next-generation Crew Exploration Vehicles (Roger, 1986). The main challenges in the development of on-board FD&P systems are the following: (i) internal gas dynamics of SRMs is highly nonlinear, (ii) there is a number of failure modes that may lead to abrupt changes of SRMs parameters, (iii) the number and types of available sensors are severely limited, as a rule only two sensors of the head pressure and acceleration, (iv) the fault detection is a complicated ill-posed inverse problem, and (v) the safe time window between the detectable onset of a catastrophic failure is typically a few seconds. These difficulties suggest that the model based approach to the IVHM of SRMs that incorporates information about physical processes underlying the nominal and off-nominal regimes can minimizes the number of "misses" and "false alarms" and reduce learning time required for accurate prediction of the fault dynamics forward in time. Preliminary numerical research (Luchinsky et al May 2007) confirms this conjecture.

Indeed, dynamical models of internal SRMs ballistics and many SRMs fault modes are well studied, see e.g. (Culick, 1996; Salita, 1989; Sorkin, 1967) and references therein. Examples of faults, for which quite accurate dynamical models can be introduced, include: (1) combustion instability; (ii) case breach fault, i.e. local burning-through of the rocket case; (iii) propellant cracking; (iv) overpressure and bursting of the case induced by nozzle blocking or bore choking. The combustion instabilities were studied in detail in the classical papers of (Culick and Yang, 1992; Culick, 1996) and (Flandro et al, 2004). Bore choking phenomenon due to radial deformation of the propellant grain near booster joint segments was studied numerically in (Dick et al., 2005; Isaac and Iverson, 2003; Wang et al., 2005) and observed in primary construction of the Titan IV (see the report, Wilson at al., 1992).

A model based fault diagnostic and prognostic system for a case breach fault in a subscale SRM was introduced in our earlier work (Smelyanskiy et al., 2005; Osipov et al., March 2007 and July 2007; Luchinsky et al., 2007 and 2008). The FD&P system in this work was based on a novel Bayesian inferential framework allowing for an analytical solution of the reconstruction problem in a stochastic nonlinear dynamical model in the presence of measurement noise. The performance of the FD&P system was verified using 2D high-fidelity FLUENT modeling and the results of the ground firing test. It was shown that the reconstructed system describes the SRMs ballistics with good accuracy.

In this paper we present an extension of the results obtained for the subscale motor to a case breach model of large segmented SRMs. The extension of this FD&P system to large segmented rockets is complicated due to the following reasons. Firstly, the effect of the mass addition from the propellant walls to the gas flow in the combustion chamber (Salita, 1989 and 2001) has to be taken into account to calculate the pressure distribution along the axis of the large rocket (Osipov et al., 2007, March). Secondly, an additional difficulty in modeling internal ballistics of the large segmented SRMs is related to the fact that the propellant burning model has to be extended by including the corrections for erosive burning and friction.

The FD&P system in multi-segment SRMs is based on our model of the internal ballistics that describes dynamics of the nominal regime as well as the off-nominal regimes in the presence of different faults, including the case breach fault. The model consists of a set of one-dimensional partial differential equations coupled to the equations of the nozzle ablation, propellant regression, erosive burning, and the dynamics of the case breach fault. The later takes into account heat transfer between the hot gas flow and hole walls, melting, and burning of the metal surface. The model is solved in a quasi-steady approximation by dividing the combustion volume into a number of ballistic elements, setting up a boundary value problem with boundaries at the head and aft of the rocket, and solving resulting boundary value problem for stationary axial distributions of the flow variables at each time step.

The FD&P system consists of the diagnostics of the fault parameters using steady-state equation for the nozzle stagnation pressure (Salita, January 1989) and prognostics of the combustion gas and fault dynamics using inferred fault parameters and solutions of the model equations forward in time or scaling algorithm (McMillin, 2006).

The PM and FD&P system are validated using results of the high-fidelity simulations in FLUENT and analysis of the time-traces obtained in the ground firing tests of a subscale motor.

The paper is organized as follows. Symbols and abbreviations are defined in the Nomenclature. The performance model is described in the Sec.2. The fault diagnostics and prognostic system for large segmented SRM is introduced in Sec. 3. The scaling algorithm for prediction of the SRM and fault parameters is outlined in Sec. 4. Finally, the conclusions are drawn in the final section.

2. PERFORMANCE MODEL

2.1 Equations of gas dynamics

The gas dynamics in the combustion chamber is determined by the system of the equations for the mass, momentum and energy conservation. Taking into account a well known result (Salita, 1989; Sorkin, 1967) that the internal ballistics of SRMs is described to a high precision by averaging hydrodynamic equations over the port area we obtain the following set of 1D partial differential equations (Smelyanskiy et al., 2005; Osipov et al., 2007, March and 2007, July; Luchinsky et al., 2007) for the gas dynamics in the combustion chamber:

$$\begin{aligned} &\partial_t A_p \rho = -\partial_x \rho u + \rho_p r_b l, \\ &\partial_t (A_p \rho u) = -\partial_x A_p (\rho u^2 + p) - p \partial_x A_p - \lambda \rho u^2 l, \\ &\partial_t (A_p \rho e_T) = -\partial_x u \left(\rho e_T + p\right) + H \rho_p r_b l, \end{aligned} \tag{1}$$

where $\partial_t \equiv \partial / \partial t$, $\partial_x \equiv \partial / \partial x$; x is the coordinate along the motor axis, and $e_t = \left(c_v T + u^2/2\right)$; $H = c_0 T_0$ is the combustion heat of the solid propellant.

Due to the high temperature T of combustion products in the combustion chamber, the hot mixed gas can be considered as a combination of ideal gases. As we are interested in average gas characteristics (head pressure and temperature) we will characterize the combustion products by averaged parameters using the state equation for an ideal gas:

$$\frac{p}{\rho} = (c_P - c_V)T = \frac{p_0}{\rho_0}\left(\frac{T}{T_0}\right) = \frac{c_0^2}{\gamma}\left(\frac{T}{T_0}\right) \tag{2}$$

2.2 Regression of propellant surface

We take into account the propellant erosion in a large segmented rocket assuming that the erosive burning rate of the propellant radius can be presented in the form

$$\dot{R} = r_b = a p^n + \dot{r}_{er} \ . \tag{3}$$

The erosive burning is taken into account in the Vilyunov's approximation

$$\dot{r}_{er} = C\left(I - I_{cr}\right) \tag{4}$$

for $I > I_{cr}$ and 0 otherwise, where C and I_{cr} are constants and $I = const\left(\rho u / r_b \rho_p\right)\mathrm{Re}^{-1/8}$, where Re is the Reynolds number.

2.3 Model of the propellant geometry

To model the actual propellant geometry along the rocket axis the combustion chamber is divided into N segments as schematically shown in Figure 1. For each segment "i" the port area $A_p(x_i)$ and perimeter $l(x_i)$ averaged over the segment length dx_i are provided in the form of the design curves (DCs)

$$A_p(x_i) = f_{Ai}(R(x_i)), \quad l(x_i) = f_{li}(R(x_i)) \tag{5}$$

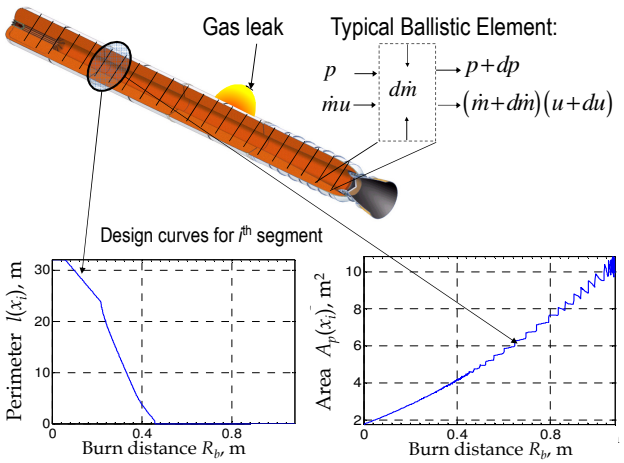

Figure 1 Sketch of a cross-section of an idealized geometry of the multi-segment RSRMV rocket and an example of the design curves (5) for the middle section.

(see Figure 1). Note that the burning area and the port volume for each segment are given by the following relations

$$dA_b(x_i) = l(x_i)dx_i, \quad dV(x_i) = A_b(x_i)dx_i, \qquad (6)$$

and, therefore, are uniquely determined by the burning rate r_{bi} for each ballistic element.
For numerical integration each segment was divided into a finite number of ballistic elements. The design curves were provided for each ballistic segment.

2.4 Model of the nozzle ablation

To model nozzle ablation we use the Bartz' approximation (Bartz, 1965; Hill and Peterson,1992; Handbook, 1973). In this approximation the ablation rate of the nozzle radius R_N is given (Osipov et al., 2007, March and 2007, July; Luchinsky et al., 2007) by the following equation:

$$\dot{R}_N = v_{t0}\left(p/p_{\max}\right)^{1-\beta}\left(R_N/R_{t,in}\right)^{-\beta}\left[\left(T-T_{abl}\right)/\left(T_t-T_{abl}\right)\right], \qquad (7)$$
$$v_{t0} = \varepsilon C_p\left(\frac{\gamma p_{\max}}{\Gamma c_0}\right)^{1-\beta}\left(\frac{2R_{t,in}}{\mu}\right)^{-\beta}\frac{\left(T_t-T_{abl}\right)}{\left[c_{ins}\left(T_{abl}-T_0\right)+q_{ins}\right]},$$

where typical values of fitting parameters are $\beta \approx 0.2$ and $\varepsilon \approx 0.023$. In a particular case of the ablation of the nozzle throat (t) and nozzle exit (ex) this approximation is reduced to

$$\dot{R}_t = v_{m,t}\left(\frac{p_0}{p_{\max}}\right)^{1-\beta}\left(\frac{R_t}{R_{t,in}}\right)^{-\beta}, \quad A_t(t) = \pi R_t^2(t), \qquad (8)$$

$$\dot{R}_{ex} = v_{m,ex}\left(\frac{p_0 A_t}{p_{\max}A_{ex}}\right)^{1-\beta}\left(\frac{R_{ex}}{R_{ex,in}}\right)^{-\beta}\frac{\left(T_{ex}-T_{abl}\right)}{\left(T_t-T_{abl}\right)}, \qquad (9)$$

where $R_{t,in}=R_t(0)$, $R_{t,in}=R_t(0)$ are initial values of the nozzle throat and nozzle exit radii and $v_{m,t}$ and $v_{m,ex}$ are constants determined by fitting experimental data. In practice, to fit experimental or numerical results on the nozzle ablation it suffices to substitute β = 0.2 into the Eqs. (8), (9) and to obtain values of $v_{m,t}$ and $v_{m,ex}$ by regression.

2.5 Model of the burning-though of a hole

To complete the model of the case breach fault for the segmented RSRMV the system of equations (1)--(6), (8), (9) above has to be extended by including equations of the hole growth model (Luchinsky et al., 2007; Osipov et al., 2007, March & July)

$$\dot{R}_h = v_h(p_{t,h},T_{h,t}) = \frac{Q_c+Q_R+Q_b}{\left[q_{met}+C_{met}\left(T_{mel}-T_{m0}\right)\right]\rho_{met}}, \qquad (10)$$

$$Q_R = \sigma\left[1-\exp\left(-\lambda p_{t,h}\right)\right]\left(T_t^4-T_{met}^4\right),$$

$$Q_c = 0.023C_p\left(\frac{\gamma p_{t,h}}{\Gamma c_0}\right)^{0.8}\left(\frac{2R_h}{\mu}\right)^{-0.2}\left(T_t-T_{met}\right), \qquad (11)$$

$$Q_b = v_{fb}\left[q_{met}+C_{met}\left(T_{mel}-T_{m0}\right)\right]\rho_m.$$

2.6 Performance model

Combining the equations of gas dynamics with the dynamics of propellant regression, nozzle ablation, and case breach fault the performance model of the large segmented SRM in the presence of faults can be summarized as follows:

$$\begin{cases} \partial_t\left(UA_p\right)+\partial_x\left(f(U)A_p\right)=S, \\ A_p(x_i)=f_{Ai}(R(x_i)), \qquad l(x_i)=f_{li}(R(x_i)), \\ \dot{R}=ap^n+C\left(I-I_{cr}\right), \\ \dot{R}_t = v_{m,t}\left(\frac{p_0}{p_{\max}}\right)^{1-\beta}\left(\frac{R_t}{R_{t,in}}\right)^{-\beta}, \\ \dot{R}_{ex} = v_{m,ex}\left(\frac{p_0A_t}{p_{\max}A_{ex,in}}\right)^{1-\beta}\left(\frac{R_{ex}}{R_{ex,in}}\right)^{-\beta}\frac{\left(T_{ex}-T_{abl}\right)}{\left(T_t-T_{abl}\right)}, \\ \dot{R}_h = \frac{Q_c+Q_R+Q_b}{\left[q_{met}+C_{met}\left(T_{mel}-T_{m0}\right)\right]\rho_{met}}, \end{cases} \qquad (12)$$

where conservative variables of the gas dynamics and function f(U) are given by the following equations

$$U = \begin{bmatrix}\rho \\ \rho u \\ \rho e_T\end{bmatrix}, \quad f(U) = \begin{bmatrix}\rho u \\ \rho u^2+p \\ \rho u e_T+up\end{bmatrix}, \qquad (13)$$

and the source terms that include fault terms at a given location x_0 have the form

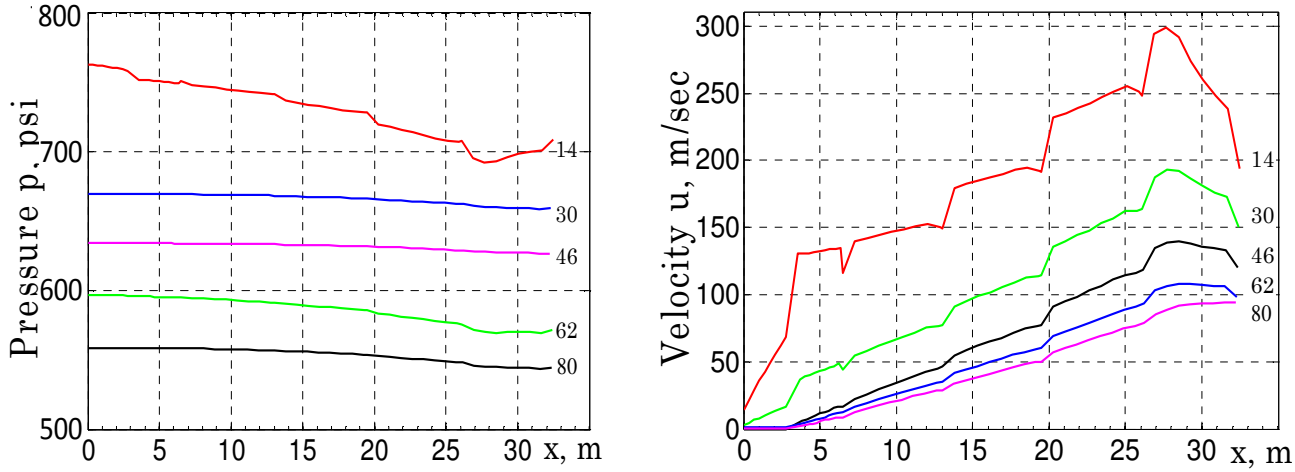

Figure 2 Nominal regime: Results of numerical solution of Eqs (17),(20) for axial distributions of pressure (left) and velocity (right) at different moments of time. Time after ignition: 14, 30, 46, 62, and 80 seconds. The value of x is measured from the motor head. The dips in the right figure for time 14 sec relate to the propellant grain boundaries.

$$S=\begin{bmatrix} \rho_p \dot{R} l(x)-\rho_{t,h}u_{t,h}A_h\delta(x-x_0) \\ p\partial_x A_p-\lambda\rho u^2 l(x) \\ H\rho_p\dot{R}l(x)-h_{t,h}\rho_{t,h}u_{t,h}A_h\delta(x-x_0)\end{bmatrix}. \quad (14)$$

Here A_h is the cross-section of burning-through hole and $u_{t,h}$ is the gas velocity through the hole. The main rocket thrust F_N and lateral (side) thrust F_h induced by the gas flow through the hole are given by

$$F_N = J_t c_0 M_{ex}\varphi_G + (p_{ex}-p_{atm})A_{ex},$$
$$F_h = J_h c_0\left(\frac{2}{\gamma+1}\right)^{1/2} + (p(x_0)-p_{atm})A_h, \quad (15)$$

where

$$J_t=\rho_t u_t A_t, \quad J_h=\rho_{h,t}u_t A_h.$$

and p_{amb} is an ambient pressure and the density $\rho_{h,t}$ at the hole throat corresponds to the hole stagnation density at the point of location of the hole.

2.7 Integration of the PM

We notice that (12) is a system of nearly balanced PDEs with slowly varying parameters. This is an example of PDEs with multiple time scales (Knoll et al., 2003), where the slower dynamical time scale is a result of a near balance between $\partial_x(f(U)A_p)$ and S in the first equation and slowly varying parameters in the last four equations in (12) The fast dynamics of (12) corresponds to the acoustic time scale. To see the multiple time scale character of the system (12) more clearly let us introduce dimensionless variables

$$p\to\frac{p}{p_0}, \rho\to\frac{\rho}{\rho_0}, \rho_p\to\frac{\rho_p}{\rho_0}, T\to\frac{T}{T_0}, R_N\to\frac{R_N}{L_0},$$
$$t\to\frac{t}{t_0}, R\to\frac{R}{L_0}, l\to\frac{l}{L_0}, A_p\to\frac{A_p}{L_0^2}, u\to\frac{u}{c_0}=M_0; \quad (16)$$

where $t_0 = L_0/ap_0^n \approx 10^{-2}$ sec; $p_0 = p_0(t=0)$, $\rho_0 = \rho_0(t=0)$ are the gas pressure and density near the rocket head at initial time point after the ignition, $M_0 = u/c_0$, $L_0 \approx 1$m are characteristics scales of time and length, $r_{p0} = ap_0^n$ is a typical burning rate. In dimensionless variables (12) can be rewritten as follows

$$\partial_x A_p\begin{bmatrix}\rho M_0 \\ \gamma p M_0^2+p \\ \rho M_0\left(T+\frac{\gamma-1}{2}M_0^2\right)\end{bmatrix} = -\varepsilon\partial_t A_p\begin{bmatrix}\rho \\ \rho M_0 \\ \rho\left(T/\gamma+\frac{\gamma-1}{2}M_0^2\right)\end{bmatrix} +$$
$$\begin{bmatrix}\varepsilon\rho_p\dot{R}l(x)+\rho_{t,h}M_{0,t}A_h\delta(x-x_0) \\ p\partial_x A_p-\gamma\lambda\rho M_0^2 l(x) \\ \varepsilon\rho_p\dot{R}l(x)+\rho_{t,h}M_{0,t}A_h\delta(x-x_0)\end{bmatrix} \quad (17)$$

Here we have introduced small parameter $\varepsilon = L_0/(t_0c_0) < 10^{-5}$ corresponding to the ratio of the characteristic velocity of the propellant surface regression ($r_{p0} \approx 10^{-2}$ m/sec) to the speed of sound ($c_0 \approx 1006$ m/sec). It is clear that in the first approximation at each given moment of time the axial distribution of the flow variables in a segmented rocket can be found in quasi-steady approximation neglecting a small last term proportional to $\varepsilon = 10^{-5}$. Note that two source terms in the 1st and 3rd Eqs. of (17) are also $\propto\varepsilon$ but these terms cannot be neglected, because they are proportional to $\rho_p \approx 10^2$.

To solve equations (17) one can neglect the last term $\propto\varepsilon$ and complete the resulting system of ODEs by a set of

boundary conditions. The calculation of the axial distribution of the flow parameters in the quasi-steady approximation can be reduced to the integration of the system of ODEs with respect to spatial coordinate *x*. To this end it is convenient to write explicitly Euler approximation of Eqs. (17) in a quasi-steady regime on a coarse-grained (in general non-uniform) lattice of axial coordinates $\{x_i: i=1,\ldots,N\}$

$$\begin{aligned}
&\rho M_0 A_p\big|_i = \rho M_0 A_p\big|_{i+1} - \delta\rho_p \dot{R} l(x) dx_i + \rho_{t,h} M_{0,th} A_h\big|_{i_h},\\
&\left(\gamma p M_0^2 + p\right) A_p\big|_i = \left(\gamma p M_0^2 + p\right) A_p\big|_{i+1} -\\
&p\left(A_p\right)\big|_i^{i+1} + \gamma\lambda\rho M_0^2 l(x) dx_i,\\
&\rho M_0 h_T A_p\big|_i = \rho M_0 h_T A_p\big|_{i+1} - \delta\rho_p \dot{R} l(x) dx_i + h_{t,h}\rho_{t,h} M_{0,th} A_h\big|_{i_h}.
\end{aligned} \tag{18}$$

where $h = \left(T + \frac{\gamma-1}{2} M_0^2\right)/H$. The last terms in the first and third equations correspond to the mass and energy losses due to the case breach fault in the i_h ballistic element. The dynamics of the case breach fault in this approximation is determined by the dynamics of the area of the case breach A_h. Note that the same model can be used to model other important fault modes in SRM. For example, the bore choking fault in the i^{th} ballistics element can be modeled by introducing fault induced changes to the port area A_p in this element; the crack dynamics can be modeled by introducing crack induced changes to an effective port perimeter $l(x)$ in the i^{th} ballistics element; the nozzle blocking can be modeled by introducing fault induced changes to the nozzle throat area A_t in the boundary conditions (20) below.

The boundary conditions at the aft end (at the outlet of the grain) are defined by the choking (sonic) conditions at the nozzle throat. The boundary conditions at the rocket head are determined by the continuity conditions of the gas flow from the propellant surface and through the port area at the rocket head. By adding to these two conditions the equation of state and the equation for the gas temperature in the combustion chamber as a function of the Mach number M_0 we obtain resulting boundary conditions at the rocket head (0) and aft (A) ends in dimensionless units as follows

$$\rho_0 M_{0,0} = \left(\frac{\delta\rho_p A_{b,0}}{A_{p,H}}\right) p_0^n, \quad T_0 = \left(1 - \frac{\gamma-1}{2} M_{0,0}^2\right), \quad p_0 = T_0\rho_0,$$

$$M_{0,A}\left(1 - \frac{\gamma-1}{2} M_{0,A}^2\right)^{\frac{1}{\gamma-1}} = \frac{A_t}{\Gamma A_A}, \quad T_A = \left(1 - \frac{\gamma-1}{2} M_{0,A}^2\right), \quad p_A = T_A\rho_A. \tag{19}$$

The conditions (19) can be reduced to

$$\begin{aligned}
&M_{0,0} = \left(\frac{\delta\rho_p A_{b,0}}{A_{p,0}}\right)\left(1 - \frac{\gamma-1}{2} M_{0,0}^2\right) p_0^{n-1},\\
&M_{0,A}\left(1 - \frac{\gamma-1}{2} M_{0,A}^2\right)^{\frac{1}{\gamma-1}} = \frac{A_t}{\Gamma A_A},\\
&p_A = \rho_A\left(1 - \frac{\gamma-1}{2} M_{0,A}^2\right).
\end{aligned} \tag{20}$$

The results of the numerical solution of the problem (18), (20) for nominal regime ($A_h=0$) are presented in Figure 2. This figure shows the resulting axial distributions of the pressure and velocity for five instances of time with the time step 16 sec (the time resolution of the solution was 0.2sec). It can be seen from Figure 2 that there is a substantial difference between the head and aft pressure due to the effect of mass addition. The difference is most significant at the initial time when the port area is the smallest and the flow velocity has the largest values along the axis. With time the port area is increasing and the difference between head and aft pressure becomes negligible. Our analysis showed that results presented in Figure 2 coincide with those obtained by the 3rd party using 2D CFD code that was verified and validated in multiple ground firing and flight tests and for many years is standard software for predicting internal ballistics of SRMs.

3 FAULT DIAGNOSTICS AND PROGNOSTICS

The model of internal ballistics of the SRM in off-nominal regimes allows one to develop and verify FD&P system for the large segmented SRMs. The FD&P system consists of two separate steps: (i) diagnosis or reconstruction of the fault parameters from the measured time-traces and (ii) prediction of fault and internal ballistic dynamics forward in time. We now describe each in more details.

3.1 Diagnostics of the fault parameters

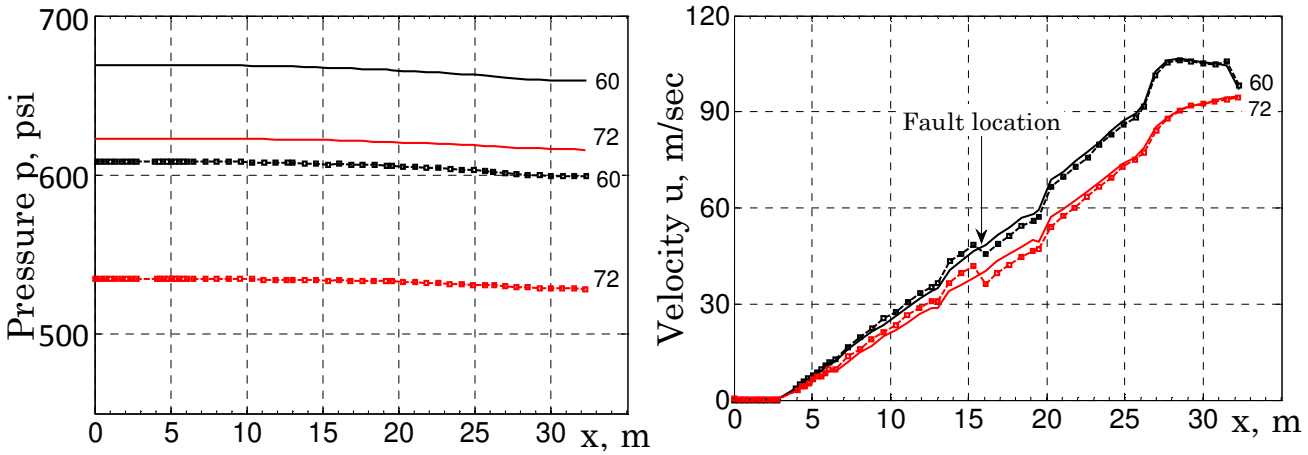

Figure 3 (left) Comparison between spatial distribution of pressure in the nominal regime (solid lines) and off-nominal regime (squares). (right). Comparison between spatial distribution of velocity in the nominal regime (solid lines) and off-nominal regime (circles). The time instants from the top to the bottom in the figure are 60 sec and 76 sec.

To be able to reconstruct fault parameters we first have to introduce a parameterization of the fault. It can be seen from the model (18) that the fault dynamics is described entirely by the dynamics of the area of the hole $A_h(t)$. The actual dynamics of the fault area can be complicated due to e.g. cracks and nontrivial geometry of the joints, see e.g. (McMillin, 2006; Smelyanskiy at al., 2008). However, analysis of the ground test results (Smelyanskiy at al., 2008) and of the challenger accident (McMillin, 2006) show that the case breach dynamics is sufficiently smooth, because it is primarily determined by the burning of the metal walls of the hole in the rocket case. It is therefore convenient to introduce a polynomial parameterization in the form:

$$A_h(t) = a_1 + a_2 t + a_3 t^2 + a_4 t^3. \qquad (21)$$

This parameterization has proved to be useful in the analysis of the ground firing test (Smelyanskiy at al., 2008). The parameters of the fault dynamics $\{a_1, a_2, a_3, a_4\}$ are reconstructed from the inferred time-series data $A_h(t)$ using the least square method. The hole is most likely to be localized at one of the section joints as shown schematically in Figure 1. As a rule, the only pressure sensor available is situated in the rocket head. Therefore, we have to verify that the measurements of the head pressure can be used to infer pressure at an arbitrary location of the hole along the rocket axis. To do so we simulate the model of internal ballistics of the SRM (18), (20) in the off-nominal regime with the case breach area given by (21) at arbitrary location. The results of such simulations for the case breach at the middle of the SRM are shown in the Figure 3. The time resolution of the calculations was 0.2 sec, initial radius of the hole $R_{h0} = 0.1$ in, burning rate of the hole wall $v_m = 0.3$ in/sec, initial time of the fault 20 sec, the fault is located in the middle section. It can be seen from the figure that the pressure drop induced by the case breach is uniform along the rocket axis. This shift practically does not depend on the location of the hole burning through the case. In particular, this result relates the shift both the head pressure to the changes in the aft pressures.

This finding allows us to use the following quasi-stationary solution for the nozzle stagnation pressure p_{ns}, which holds with good accuracy for large SRMs (Salita, 1989; McMillin, 2006):

$$p_{ns} = p_c \left[\frac{\Gamma c_0 \rho_p r_c}{\gamma p_c} \left(\frac{A_{b,eff}(t)}{A_t(t) + A_h(t)} \right) \right]^{\frac{1}{1-n}}. \qquad (22)$$

This equation is derived from the balance condition between the choked flow through the nozzle throat and the combustion gas flow from the burning surface of the grain. It relates the nozzle stagnation pressure to the burning area $A_{b,eff}$ divided by the effective area of the nozzle throat. It allows for reconstruction the effective area of the nozzle throat from the time-traces of the nozzle stagnation pressure.

To see this we notice that burning area $A_b(R(t))$ and nozzle throat area $A_t(t)$ are determined by the known initial condition and measured time-traces of the gas pressure $p_{ns}(t)$. The accuracy of the relation (22) is further improved by introducing the effective burning area $A_{b,eff}(R(t))$ in the nominal regime. Indeed, in the nominal regime $A_h(t) = 0$ while $p_{ns}(t)$ and $A_t(t)$ are well known. This allows one to determine uniquely the effective burning area $A_{b,eff}(R(t))$ as a function of the burn distance $R(t)$. This functional dependence is assumed to be valid in the off-nominal regime of the case breach. Therefore, one

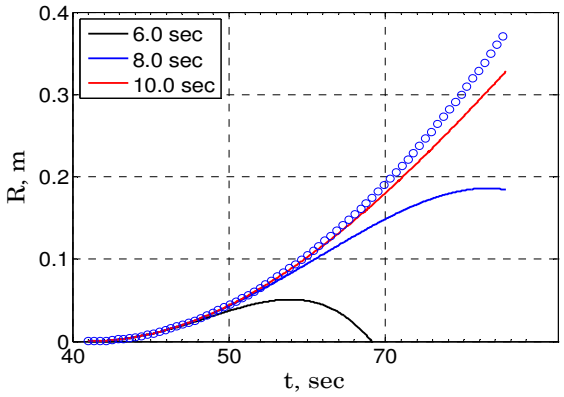

Figure 4 The time-trace of the actual hole dynamics (blue open circles) as compared with the results of the predictions using model (21) for three different times of inference: 6 sec after the fault, 8 sec, and 10.0 sec.

can use data of the pressure sensor at the rocket head to estimate the deviations of the nozzle stagnation pressure p_{ns} from the nominal regime and subsequently to use equation (22) to estimate the area of the case breach fault $A_h(t)$ according to the following algorithm:

1) Use the nominal regime time-traces to determine the effective burning area by Eq. (22)
$$A_{b,eff}(t) = \left[\frac{\gamma A_t(t)}{\Gamma c_0 \rho_p a}\right] p_{ns}^{1-n}(t);$$
2) Use measured time-trace of the head pressure in the off-nominal regime $p_H(t)$ to find fault-induced pressure at the aft end using the fact that the pressure changes induced by the fault are uniform along the motor axis
$$p_A^{(fault)}(t) = p_A^{(nom)}(t) + \left(p_H^{(fault)}(t) - p_H^{(nom)}(t)\right);$$
3) Use nominal time-trace of the Mach number at the aft end to determined nozzle stagnation pressure
$$p_{ns}^{(fault)}(t) = p_A^{(fault)}(t)\left(1 - \frac{\gamma-1}{2} M_{A,0}^2(t)\right)^{-1};$$
4) Use Eq. (22) to determined time-trace of the hole area
$$A_h(t) = \left[\frac{\Gamma c_0 \rho_p a A_{b,eff}(t)}{\gamma\left(p_{ns}^{(fault)}(t)\right)^{1-n}}\right] - A_t(t).$$

The parameters of the fault dynamics $\{a_1, a_2, a_3, a_4\}$ are reconstructed from the inferred time-series data $A_h(t)$ using the least square method. We can now use the values of the parameters $\{a_i\}$ reconstructed during the diagnostic to predict fault and internal ballistics of the SRM forward in time.

3.2 Prognostics of the fault parameters: FD&P algorithm

We note that the values of the reconstructed parameters a_i of Eq. (22) depend on the diagnostics time. The convergence of the forward predictions also depends on the diagnostic time, which is, therefore, one of the key characteristics of the FD&P system. The convergence of the predicted hole area time-traces towards actual time-traces of $A_h(t)$ is illustrated in Figure 4. In this test the fault initialization time iss 40 sec, the hole area measurements are assumed to have sampling rate 1kHz and measurement noise 1%. The filtering procedure is used to reduce the noise in the data. The time intervals ΔT_m used to infer fault parameters are 8 sec and 11 sec. The predictions are made up to 85 sec of the flight. Note that the convergence of the predictions of the hole area is achieved approximately after 10 sec of diagnostics. The inferred values of a_i can now be used to predict the case breach dynamics forward in time.

The mean values and standard deviations of the parameters $\{a_i\}$ reconstructed during diagnostics of the inferred time-series data $A_h(t)$ can now be used to integrate model of internal ballistics (12) forward in time to obtain predictions of the pressure and thrust dynamics in the presence of the fault. The results of the predictions for the nozzle and side thrust are shown in the Figure 5. In this test the fault was located at the middle of the motor and initial time T_f = 45 sec. In the figures the predictions are made for two different time intervals of diagnostic: (i) ΔT_m=8 sec (left) and (ii) ΔT_m=12 sec (right). The beginning and the end of the time interval used to infer fault parameters are indicated by red vertical lines. The

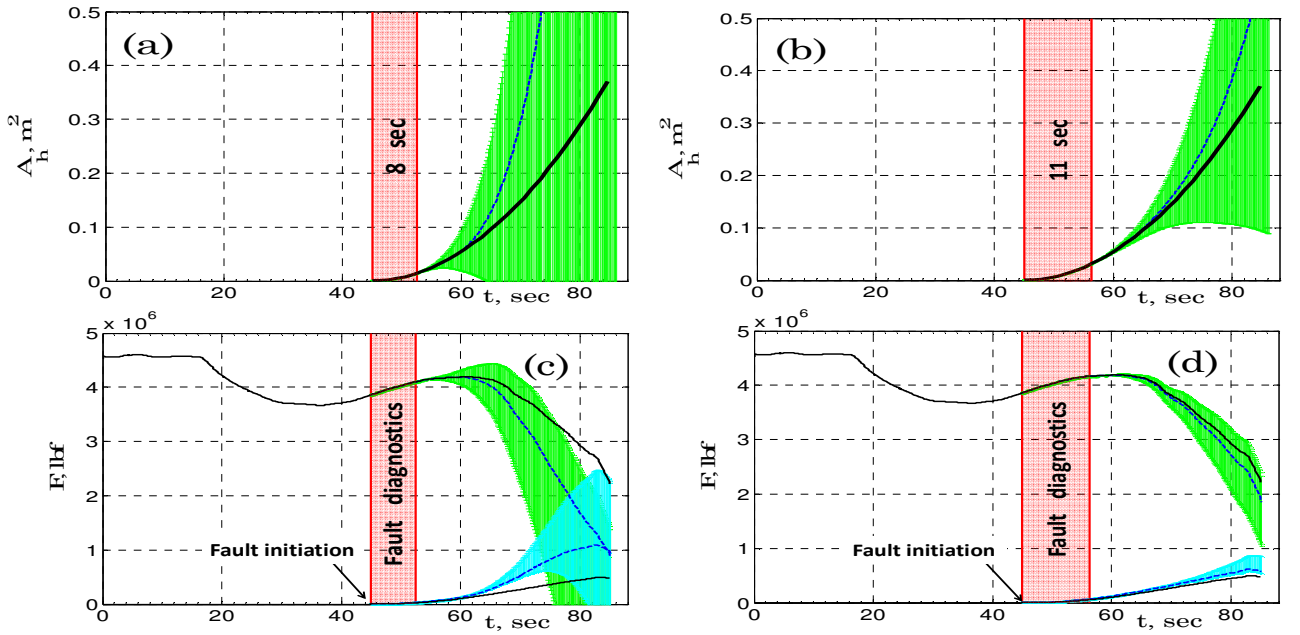

Figure 5 Convergence of the predicted hole area (top) and thrust (bottom). The actual time-traces (black solid lines) obtained by the integration of the performance model are compared with the time-traces of mean predicted values (blue dashed lines). The green shading indicates standard deviations for the predicted values of area and nozzle thrust. The cyan shading indicates standard deviations for predicted value of the side thrust.

metal burning rate corresponding to the hole radius growth rate is 0.3 in/sec. We take the initial radius of the hole equal to 0.1in. It can be seen from the figure that the predictions begin to converge after 12 sec.
We note, however, that full integration of the model forward in time is time consuming procedure and it is desirable to reduce the time of calculations required for prediction. This can be achieved by applying for predictions scaling algorithm based on earlier results of (McMillin, 2006).

4 SCALING ALGORITHM FOR FAULT PROGNOSTICS

This scaling algorithm (McMillin, 2006), unlike FD&P algorithm presented above, requires a knowledge of the time-trace of the pressure in the nominal regime. Since this requirement is a necessary prerequisite for the space flight one can substantially reduce the prediction time. Let us remind briefly main steps of the scaling algorithm (McMillin, 2006). The key assumption based on extensive experimental results is that the empirical coefficient q

$$q = \frac{\partial \ln(C^*)}{\partial \ln(p)} = const, \qquad C^* = \frac{p^{1-n} A_t}{A_s \rho_p a}. \tag{23}$$

is constant. Here $C^* = pA_t / \dot{m}$ is characteristic exhaust velocity and $\dot{m} = A_b \rho_p R = A_b \rho_p a p^n$ is the mass flow with total burning area A_b, where the burning law is given by $R = ap^n$. To see more clearly the meaning of (23) we write its solution on a discrete time lattice $\{t_i: i=1,\ldots,N\}$ chosen in such a way that every moment of time in the nominal t_{Ni} and off-nominal t_{Di} regimes correspond the same fixed lattice of burned distances $\{r_i: i = 1,\ldots,N\}$ and therefore the burning area $A_{s,i}$ at any given instant of time is also the same

$$C_i^* p_i^{-q} = \frac{p_i^{1-n-q} A_{t,i}}{A_{s,i} \rho_p a} = const \tag{24}$$

The experiments and numerical simulation show that the later expression is constant with good accuracy during the steady burn out of the propellant both in nominal (N) and off-nominal, deviant (D), regimes. We notice that the mean value of q is approximately 0.007, i.e. 2 orders of magnitude less than $(1-n) = 0.7$ and can be neglected in the calculations.
Using Eq. (24) for the nominal p_{Ni} and off-nominal p_{Di} pressures at the instant t_i on a given time lattice $\{t_i\}$ we obtain

$$p_{Di} = p_{Ni} \left(A_{t,Ni} / A_{t,Di} \right)^{\frac{1}{1-n-q}}, \tag{25}$$

where $A_{t,Ni}$ and $A_{t,Di}$ are nozzle throat area in the nominal regime and the nozzle effective area in the off-nominal regime at the instant t_i on the nominal time lattice $\{t_i\}$ and instant t_{Di} on the deviant time lattice $\{t_{Di}\}$ as explained in the next sub-section. It was noticed that if the lattice of burned distances $\{r_i\}$ is kept the same in nominal and off-nominal regimes the corresponding time lattices $\{t_i\}$ in these two regimes will be different. To find the scaling of the time lattice the burning law is used as follows (McMillin, 2006)

$$\Delta r_i = r_i - r_{i-1} = a p_{Ni}^n \Delta t_{Ni} = a p_{Di}^n \Delta t_{Di} \quad \text{or}$$

$$\Delta t_{Di} = \Delta t_{Ni} \left(p_{Ni} / p_{Di} \right)^n. \tag{26}$$

Therefore, the time scale in the presence of the fault is

$$t_{D,i} = t_{D,i-1} + \Delta t_{Di}. \tag{27}$$

Finally, substituting (25) into (26) we have

$$\Delta t_{Di} = \Delta t_{Ni} \left(A_{t,Ni} / A_{t,Di}^e \right)^{\frac{-n}{1-n-q}}. \tag{28}$$

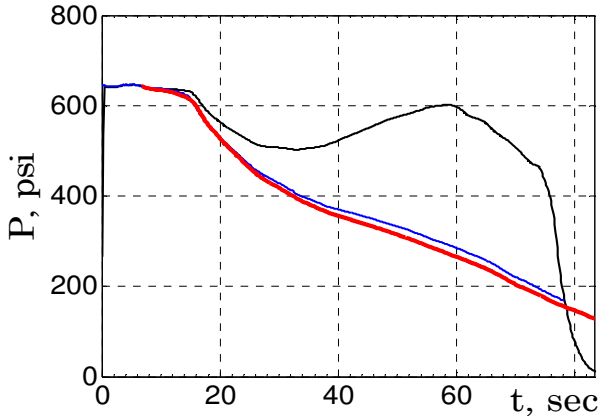

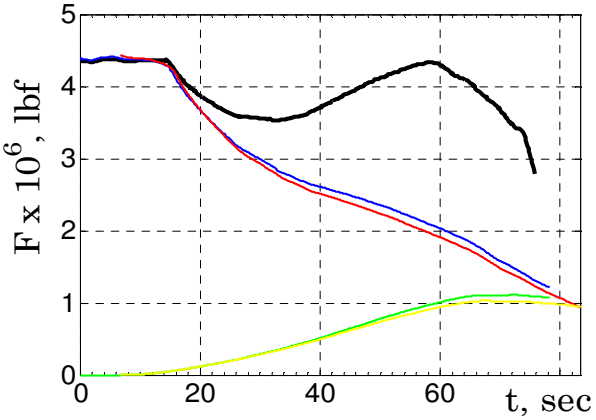

Figure 6 (left) Nozzle pressure (black line) in the nominal regime are compared with the calculations of the fault induced pressure using 1D model (blue line) and scaling algorithm (red line). (right) Nozzle vacuum thrust (black line) in the nominal regime as compared to the deviation of the thrust from nominal regime calculated using scaling algorithm (red line) and 1D model (blue line). The hole' thrust calculated using scaling equations (green line) and 1D algorithm (yellow line).

Fault dynamics can be given in any form, in particular it is a given function of time (McMillin, 2006)

$$A_{h,i} = f(t_{D,i} - t_f). \tag{29}$$

The effective nozzle throat area for the case breach fault $A^e_{t,D}$ is the sum of the hole area A_h in the case and of the slightly modified nozzle throat area $A_{t,D}$

$$A^e_{tD,i} = A_{h,i} + A_{tD,i}. \tag{30}$$

To calculate nozzle thrust the empirical constant thrust coefficient was used (McMillin, 2006)

$$C_F = F_N / pA_{t,N}, \qquad C_{F,N} = C_{F,D}. \tag{31}$$

If combined with (25) the following result for the deviant nozzle thrust F_{Di} can be obtained

$$F_{Di} = F_{Ni} = \left(\frac{A_{t,Di}}{A_{t,Ni}}\right)\left(\frac{A_{t,Ni}}{A^e_{t,Di}}\right)^{\frac{1}{1-n-q}}. \tag{32}$$

Eq. (15) can be used to calculate the side breach thrust . The resulting expression for the side vacuum thrust (p_{amb} = 0) can be simplified

$$F_h = p_0 A_h \left(\frac{2}{\gamma+1}\right)^{\frac{\gamma}{\gamma-1}}(\gamma+1). \tag{33}$$

The algorithm suggested in earlier work (McMillin, 2006) consists of iteration of Eqs. (27)-(30) until convergence of Δt_i is achieved. On substituting Eq. (29) into Eq. (30) and Eq. (30) into Eq. (28) the equations. (27)-(30) can be reduced to two equations in the form

$$\Delta t_{Di} = \Delta t_{Ni}\left(\frac{A_{t,i}}{A_{tD,i} + f(t_{D,i} - t_f)}\right)^{\frac{-n}{1-n-q}}, \tag{34}$$

$$t_{D,i} = t_{D,i-1} + \Delta t_{Di}.$$

where t_{Di} is given by (27). There are three unknown variables $\{\Delta t_{Di}, A_{tDi}, t_{Di}\}$ in two Eqs. (34), therefore one more equation is needed to implement iterative procedure. We use the assumption (McMillin, 2006) that the nozzle throat area is only a function of time $A_{tD}(t_{Di}) = A_{tN}(t_{Di})$, which holds for actual rocket parameters.

We now verify of both algorithms by direct comparison of their performance in an off-nominal regime with the fault initial time 10 sec and initial hole radius 0 in. The results of the calculation of pressure, nozzle and side thrusts using model integration and scaling equations are shown in the Figure 6. The results of the simulations of the pressure and nozzle thrust of the SRM in the off-nominal regime are shown by the blue dotted lines. The results of the fault-induced scaling of the nominal time-traces of pressure and nozzle thrust are shown by the red and cyan dashed lines respectively. The maximum relative deviation of the scaling algorithm results from the simulation results is less than 7%. However, the safety margins do not allow for the deviation of the nozzle thrust more than 10% of the nominal regime. Within these safety margins the agreement between the predictions based on the scaling algorithm results and on simulations is better than 1%. The reason for the small deviation of the scaling algorithm from the results of model integration

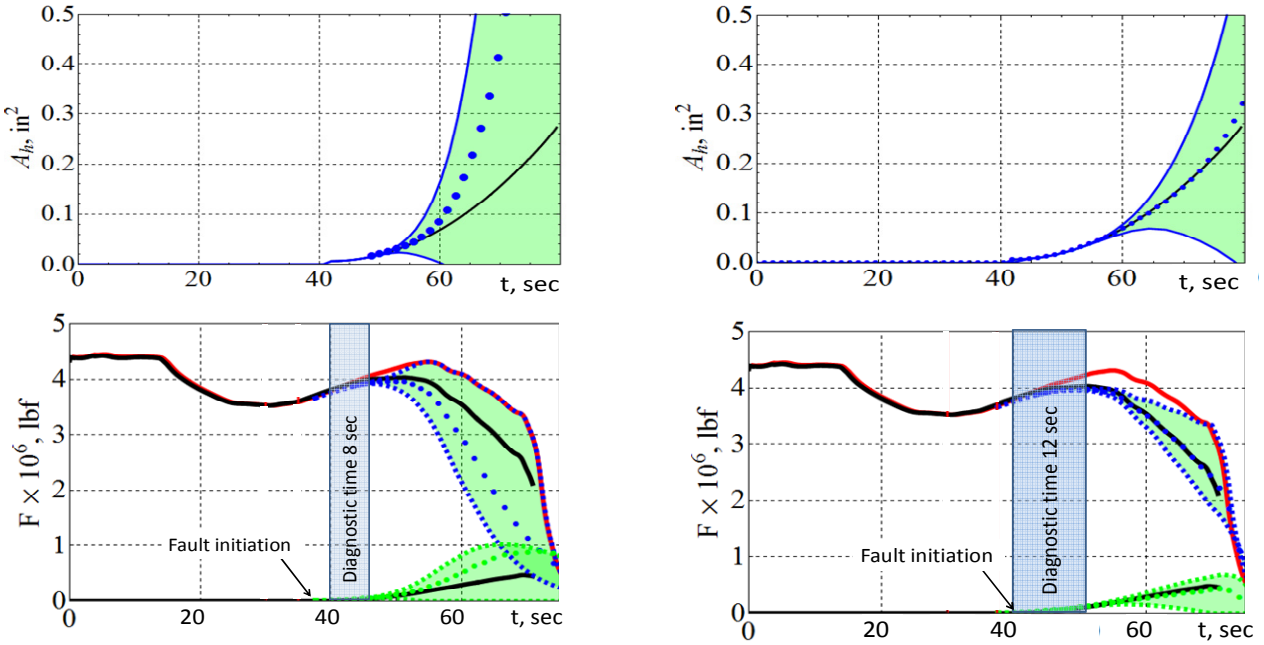

Figure 7 Convergence of the predicted hole area (top) and thrust (bottom). The actual time-traces (black solid lines) are compared with the time-traces of mean predicted values of nozzle thrust (blue dotted lines) and side thrust (green dotted lines). The green shading indicates standard deviations for the predicted values of area and nozzle thrust. The nozzle thrust in nominal regime is shown by red lines.

is that scaling algorithm ablation of the nozzle throat area, while chamber pressure and nozzle thrust are slightly underestimated. The modeling of the nozzle ablation in the scaling algorithm will be improved in the next version of the code.

Note also that the nominal regimes are well established for on-board FD&P and full simulations of the internal ballistics are not necessary. Therefore, it becomes possible to use simplified predictions based on the scaling equations for the prognostics of the case breach fault. The later algorithm is much faster than full simulations of the model. For example the full simulation takes about 58 sec on the laptop with dual core Intel processor, while scaling of the given time-traces takes less than 0.3 sec. The results of the prognostics based on the scaling equations are presented in Figure 7. In the figures the predictions are made for two different time intervals of diagnostic: (i) ΔT_m=8 sec (left) and (ii) ΔT_m=12 sec (right). The beginning and the end of the time interval used to infer fault parameters are indicated by red vertical lines. Fault initial time T_f = 30 sec in all cases, initial hole radius 0 in, metal burning rate 0.3 in/sec.

We therefore conclude that it is possible to perform in-flight fault diagnostics and prognostics of the case breach fault in large segmented SRMs using only measurements of the head pressure in the combustion chamber. For realistic fault parameters, sufficiently smooth dynamics of the fault and relatively low measurement noise the convergence of the predictions can be achieved after 10 seconds of the fault diagnostics.

Note that the dispersion of predictions for the pressure and thrust is smaller than the dispersion of the corresponding predictions for the area of the case breach. The reason is that the fault is most likely to occur in the second half of the flight of the first stage and the prediction time corresponds to the decreasing part of the time-trace of the head pressure. This will result in the decreasing of the dispersion of the pressure predictions according to the Eq. (25)

$$p_{Di} = p_{Ni}\left(\frac{A_{t,Ni}}{A_{t,Di}+A_h}\right)^{\frac{1}{1-n-q}}.$$

One can see from this equation that despite the fact that the dispersion of the hole area (A_h) predictions in the denominator is growing, the dispersion of the predictions of the deviant pressure p_{Di} is decreasing together with decreasing of the nominal pressure p_{Ni}.

5 CONCLUSION

We analyze the problem of in-flight diagnostics and prognostics of the SRM failure modes and, in particular, of the case breach fault. To model the internal ballistics of large segmented SRMs we introduce a 1D time accurate model that takes into account geometry of the grain, the propellant regression rate, including erosive burning and surface friction, nozzle ablation, and the case breach dynamics. The model is integrated in quasi-steady approximation by solving the boundary value problem using shooting method. The results of integration were verified by comparison with 2D FLUENT simulations (developed by the third party). The diagnostics of the case breach dynamics is performed using stationary solution for the nozzle stagnation pressure and the measurements of head pressure using polynomial approximation of the hole area dynamics and least square method to infer coefficients of the polynomial. We demonstrate next that it is possible to perform in-flight fault diagnostics and prognostics of the case breach fault in large segmented SRMs using only measurements of the head pressure in the combustion chamber. Prognostics are developed using both integration the model equations forward in time and using scaling equations (McMillin, 2006). The results of predictions based on scaling equations are in good agreement with the results of the integration of the 1D model in off-nominal regime. The method can be applied to the analysis of a number of other faults in SRMs.

REFERENCES

D.R. Bartz. (1965), *Heat Transfer from Rapidly and from Heated Air*, in Advances in Heat Transfer, vol. 2, Hartnett, J. P. , and Irvine, T. F. Jr., eds., New York: Academic Press.

W. A. Dick et al. (2005, July), Advanced Simulation of Solid Propellant Rockets from First Principles", Center for Simulation of Advanced Rockets, University of Illinois, *in Proceeding of 41st AIAA Joint Propulsion Conference & exhibit*, Tucson, Arizona.

F. E. C. Culick and V. Yang. (1992), Prediction of the Stability of Unsteady Motions in Solid Propellant Rocket Motors, Nonsteady Burning and Combustion Stability of Solid Propellants, edited by L. De Luca, E. W. Price, and M. Summerfield, Vol. 143, Progress in Astronautics and Aeronautics, AIAA, Washington, DC, pp. 719–779.

F. E. C. Culick. (1996), *Combustion of the Stability in Propulsion Systems, Unsteady Combustion*, Kluwer Academic Publisher.

G. A. Flandro *et al*. (2004, July), "Nonlinear Rocket Motor Stability Prediction: Limit Amplitude, Triggering, and Mean Pressure Shift", *in Proceeding of AIAA 2004-4054, 40th AIAA Joint Propulsion Conference & Exhibit*, Florida.

D. A. Knoll, L. Chacon, L. G. Margolin, V. A. Mousseau. (2003), On balanced approximations for time integration of multiple time scale systems", J. Comput. Phys., 185(2), pp 583-611.

P. Hill and C. Peterson (1992), *Mechanics and Thermodynamics of Propulsion,* 2-rd ed., Addison-Wesley Publishing Company, Inc. New York.

F.P. Incropera and D. P. DeWitt (2002), *Introduction to Heat Transfer*, John Wiley & Sons, NY,

D. A. Isaac and M. P. Iverson. (2003), "Automated Fluid-Structure Interaction Analysis", ATK Thiokol Propulsion, A Division of ATK Aerospace Company.

D.G. Luchinsky, V.N. Smelyanskiy, V.V. Osipov, and D. A. Timucin, and S. Lee. (2007) , "Data management and decision support for the in-flight SRM", *in*

Proceeding of AIAA-2007-2829 AIAA Infotech@Aerospace 2007 Conference and Exhibit, Rohnert Park, California.

D.G. Luchinsky, V.V. Osipov, V.N. Smelyanskiy, D.A. Timucin, D. S. Uckun. (2008), "Model based IVHM system for the solid rocket booster", *in Proceeding of Aerospace Conference, 2008 IEEE, 1-8, BigSky, Montana, 2008 Page(s):1 – 15*

D.G. Luchinsky, V.V. Osipov, V.N. Smelyanskiy, D.A. Timucin, S. Uckun, B. Hayashida, M. Watson, J. McMillin, D. Shook, M. Johnson, S. Hyde. (2009), "Fault Diagnostics and Prognostics for Large Segmented SRMs", *in Proceeding of 2009 IEEE Aerospace Conference,* Big Sky, Montana.

J. E. McMillin. (2006, July), AIAA 2006-5121, *in Proceeding of 42nd AIAA/ASME/SAE/ASEE Joint Propulsion Conference & Exhibit* , Sacramento, CA.

V. V. Osipov, D. G. Luchinsky, V. N. Smelyanskiy, S. Lee, C. Kiris, D. Timucin. (2007, March*)*, "Bayesian Framework for In-Flight SRM Data Management and Decision Support", *in Proceeding of IEEE 2007 Aerospace Conference,* Big Sky.

V.V. Osipov, D.G. Luchinsky, V.N. Smelyanskiy, C. Kiris, D.A. Timucin, S.H. Lee. (2007, July) , In-Flight Failure Decision and Prognostic for the Solid Rocket Buster, *in Proceeding of AIAA-2007-5823, 43rd AIAA/ASME/SAE/ ASEE Joint Propulsion Conference and Exhibit,* Cincinnati, OH.

Rogers (1986). Rogers Commission report. Report of the Presidential Commission on the Space Shuttle Challenger Accident

M. Sailta. (*1989*, January), "Verification of Spatial and Temporal Pressure Distribution in Segmented Solid Rocket Motors," *in Proceeding of AIAA paper 89-0298, 27th Aerospace Science Meeting,* Reno, Nevada.

M. Salita. (*1989*, July), "Closed-Form Analytical Solutions for Fluid Mechanical, Thermochemical, and Thermal Processes in Solid Rocket Motors", *in Proceeding of AIAA 98-3965,34th Joint Propulsion Conference, Cleveland.*

M. Salita. (2001), "Modern SRM ignition transient modeling. I - Introduction and physical models", *in Proceeding of AIAA-2001-3443, AIAA/ASME/SAE/ASEE Joint Propulsion Conference and Exhibit, 37th*, Salt Lake City, U.

J.C. Santiago. (1995), "An experimental study of the velocity field of a transverse jet injected into a supersonic crossflow", Ph.D. thesis, University of Illinois, Urbana-Champaign.

A. H. Shapiro. (1953.), "The Dynamics and Thermodynamics of Compressible Fluid Flow", Ronald Press, NY, vol. I ,

E. Sorkin. (1967), Dynamics and Thermodynamics of Solid-Propellant Rockets, *Wiener Bindery Ltd.*, Jerusalem.

V.N. Smelyanskiy, D.G. Luchinsky, V.V. Osipov, D.A. Timucin, S. Uckun, B. Hayashida, M. Watson, J. McMillin, D. Shook, M. Johnson, S. Hyde. (2008, December), Analysis of experimental time-traces of the ground firing test of a subscale srm with gas leak in the forward closure", *in Proceeding of 6th Modeling and Simulation / 4th Liquid Propulsion / 3rd Spacecraft Propulsion Joint Subcommittee Meeting,* Orlando, Florida.

V.N. Smelyanskiy, D.G. Luchinsky, V.V. Osipov, D.A. Timuchin, S.Uckun. (2008, July*)*, "Development of an on-board failure diagnostics and prognostics system for Solid Rocket Booster", *in Proceeding of 44rd AIAA/ASME/SAE/ASEE Joint Propulsion Conference & Exhibit, Hartford, CT.*

V.N. Smelyanskiy, D.G. Luchinsky, V.V. Osipov, D.A. Timucin, S. Uckun, B. Hayashida, M. Watson, J. McMillin, D. Shook, M. Johnson, S. Hyde. (2008a, December*)* , "Fault diagnostic and prognostic system for a gas leak fault in subscale SRM: modeling and verification in a ground firing test", *in Proceeding of 6th Modeling and Simulation / 4th Liquid Propulsion / 3rd Spacecraft Propulsion Joint Subcommittee Meeting,* Orlando, Florida.

V.N. Smelyanskiy, D.G. Luchinsky, V.V. Osipov, D.A. Timucin, S. Uckun, B. Hayashida, M. Watson, A. Ridnour, D. Shook, M. Johnson, S. Hyde. (2008b, December*)*, "Modeling, Diagnostics and Prognostics of Nozzle failures from Ground Tests Hybrid Motor Test Data", *in Proceeding of 6th Modeling and Simulation / 4th Liquid Propulsion / 3rd Spacecraft Propulsion Joint Subcommittee Meeting*, Orlando, Florida.

D.S. Stewart; K.C. Tang; S. Yoo; Q. Brewster; I.R. Kuznetsov. (2006). Multiscale Modeling of Solid Rocket Motors: Computational Aerodynamic Methods for Stable Quasi-Steady Burning, *Journal of Prop and Power,* Vol. 22, no. 6, 1382-1388.

W.G. Wilson, J.M. Anderson, and M.V. Meyden (1992, July), "Titan IV SRMU PQM-1 Overview", *in Proceeding of AIAA/ 92-3819, AIAA 28th Joint Propulsion Conference and Exhibit*, Nashville, TN.

W.G. Wilson, J. M. Anderson, M. Vander Meyden (1992, July). "Titan IV SRMU PQM-1 Overview", AIAA paper 92-3819, *in Proceeding of AIAA/SAE/ASME/ASEE, 28th Joint Propulsion Conference and Exhibi,* Nashville, TN.

Dr. **Dmitry G. Luchinsky** is a senior research scientist in MCT Inc. He obtained his MSc and PhD in physics in Moscow working on nonlinear optics of semiconductors. He is an author of more than 100 publications. He has been on a number of occasions a Royal Society Visiting Fellow and a NASA visiting scientist. He worked as a senior scientific researcher in VNII for Metrological Service (Moscow, Russia) and as a Senior Research Fellow in Lancaster University (Lancaster, UK). His research interests include nonlinear

optics, stochastic and chaotic nonlinear dynamics, dynamical inference, fluid dynamics, ionic motion. His research is currently focused on theory and CFD of gas dynamics and fluid structure interaction in SRBs.

Dr. **Viatcheslav (Slava) V. Osipov** is a leading research scientist in MCT working at NASA Research Centre on nonlinear spatial extended systems far from equilibrium with application to semiconductor physics and hydrodynamics. Slava Osipov received MS, Engineer-Physicist followed by Ph.D. and Sci. Doc. in Physics of non-equilibrium systems" (1975) from Moscow Institute of Physics and Technology (MIPT) for the study of self-organization phenomena in physical, chemical, and biological system. He was a professor in MIPT and a science-director of the Department of Fundamental Research and Theoretical Physics in Russian State Science Center "ORION", Moscow, Russia. Dr. Osipov has published 4 books and more than 250 science articles in the leading physical journals. He have worked a research professor in scientific laboratories of different countries, including in Consejo Superior de Investigaciones Cientificas, Madrid, Spain, in University of New South Wales (UNSW), Sydney, Australia, and in Hewlett-Packard Labs, CA, USA.

Dr. **Vadim N Smelyanskiy** leads the physics modeling group in Computation Science Division at NASA Ames Research Center. He has obtained his BS, MS, and PhD in Institute of Semiconductors (Kiev, Ukraine). He has worked as a consultant and research Scientist in Los Alamos National Lab., Departments of Physics in Ann Arbor, MSU, and Princeton. Currently his research interest include nonlinear dynamics, statistical mechanics, Bayesian Statistics, nonlinear modeling, computer vision, quantum, computer, fluid dynamics of solid rocket motors, nonlinear dynamics of CMG.